Virology 531 (2019) 57–68

Contents lists available at ScienceDirect

Virology

journal homepage: www.elsevier.com/locate/virology

Macropinocytosis contributes to hantavirus entry into human airway epithelial cells

Giulia Torriani[a], Jennifer Mayor[a,d], Gert Zimmer[b,c], Stefan Kunz[a,*], Sylvia Rothenberger[a,d,*], Olivier Engler[d,**]

[a] Institute of Microbiology, University Hospital Center and University of Lausanne, Rue du Bugnon 48, CH-1011 Lausanne, Switzerland
[b] Institute of Virology and Immunology (IVI), CH-3147 Mittelhäusern, Switzerland
[c] Department of Infectious Diseases and Pathobiology, Vetsuisse Faculty, University of Bern, CH-3012 Bern, Switzerland
[d] Spiez Laboratory, CH-3700 Spiez, Switzerland

ARTICLE INFO

Keywords:
Hantavirus
Viral entry
Endocytosis
Macropinocytosis
Tropism
Signaling

ABSTRACT

Hantaviruses are emerging rodent-borne negative-strand RNA viruses associated with severe human diseases. Zoonotic transmission occurs via aerosols of contaminated rodent excreta and cells of the human respiratory epithelium represent likely early targets. Here we investigated cellular factors involved in entry of the pathogenic Old and New World hantaviruses Hantaan virus (HTNV) and Andes virus (ANDV) into human respiratory epithelial cells. Screening of a kinase inhibitor library using a biocontained recombinant vesicular stomatitis virus pseudotype platform revealed differential requirement for host kinases for HTNV and ANDV entry and provided first hints for an involvement of macropinocytosis. Examination of a selected panel of well-defined inhibitors of endocytosis confirmed that both HTNV and ANDV enter human respiratory epithelial cells via a pathway that critically depends on sodium proton exchangers and actin, hallmarks of macropinocytosis. However, HTNV and ANDV differed in their individual requirements for regulatory factors of macropinocytosis, indicating virus-specific differences.

1. Introduction

Hantaviruses are emerging rodent-borne negative-strand RNA viruses associated with severe human diseases and merit significant attention as important public health problems (Jonsson et al., 2010; Krautkramer and Zeier, 2014; Krautkramer et al., 2013; Manigold and Vial, 2014; Vaheri et al., 2013b). The prototypic Hantaan virus (HTNV) and Seoul virus (SEOV) are widespread in Asia where they cause hemorrhagic fever with renal syndrome (HFRS) reaching 15% case-fatality. The New World hantaviruses Sin Nombre (SNV) and Andes (ANDV) are associated with hantavirus cardiopulmonary syndrome (HCPS) in the Americas with up to 40% mortality. Hantaviruses are currently the most important emerging viruses in Europe, including Puumala virus (PUUV) endemic in Northern Europe and Dobrava-Belgrade virus (DOBV) in the Balkans (Vaheri et al., 2013a). While PUUV causes *nephropathia endemica,* a milder form of HFRS, DOBV manifests with more severe clinical disease. The lack of a licensed vaccine and the limited therapeutic options make the development of novel antiviral strategies against hantaviruses an urgent need.

Rodents represent the natural reservoir of hantaviruses but insectivores such as shrews, moles and bats can also carry these viruses which cause asymptomatic persistent infections in these hosts. Zoonotic transmission occurs via aerosols of contaminated rodent excreta (Hansen and Nichols, 2009; Vaheri et al., 2013a, 2013c) and cells of the human respiratory epithelium represent likely early targets. After initial replication at the site of entry, hantaviruses can enter the bloodstream and disseminate systemically. In cases of severe infection, viral antigen is detectable in dendritic cells, macrophages, lymphocytes, and in microvascular endothelial cells, whose functional perturbation contributes to the fatal shock syndrome (Manigold and Vial, 2014; Muranyi et al., 2005; Vaheri et al., 2013b).

Several candidate cellular receptors have been shown to interact with glycoproteins of hantaviruses, in particular protocadherin-1 (PCDH1), αvβ3 integrin, decay-accelerating factor (DAF), and components of the complement system (Gavrilovskaya et al., 1999, 1998; Jangra et al., 2018; Krautkramer and Zeier, 2008; Popugaeva et al., 2012; Raymond et al., 2005). Recent studies demonstrated that PCDH1 is essential for entry of New World hantaviruses into vascular

* Correspondence to: Institute of Microbiology, Lausanne University Hospital, Lausanne CH-1011, Switzerland.
** Corresponding author.
E-mail addresses: Stefan.Kunz@chuv.ch (S. Kunz), Sylvia.Rothenberger-Aubert@chuv.ch (S. Rothenberger), olivier.engler@babs.admin.ch (O. Engler).

https://doi.org/10.1016/j.virol.2019.02.013
Received 3 December 2018; Received in revised form 20 February 2019; Accepted 20 February 2019
Available online 21 February 2019
0042-6822/

endothelial cells in vitro and in vivo and plays a crucial role in the pathogenesis of HCPS. Upon attachment to their receptor(s), hantaviruses are internalized by receptor-mediated endocytosis and undergo membrane fusion in acidified endosomes (Albornoz et al., 2016). An initial report demonstrated HTNV cell entry via clathrin-mediated endocytosis (Jin et al., 2002), whereas uptake of ANDV can occur independently of clathrin (Ramanathan and Jonsson, 2008). Several lines of evidence support the notion that cell entry of HTNV and ANDV critically depends on membrane cholesterol (Kleinfelter et al., 2015; Krautkramer and Zeier, 2008; Petersen et al., 2014; Tischler et al., 2005). A recent study combining an RNA interference (RNAi) silencing screen with functional assays revealed that ANDV can use multiple routes of endocytosis to enter primary human endothelial cells (Chiang et al., 2016). However, the cellular entry pathway(s) used by pathogenic hantaviruses to infect human respiratory epithelial cells remain largely unknown. In the present study, we combined an unbiased screen using a library of well-characterized kinase inhibitors covering major cellular signaling pathways with a selected panel of inhibitors of endocytosis to perform a comparative analysis of HTNV and ANDV entry into human respiratory epithelial cells. Our data provide first evidence for a role of macropinocytosis in hantavirus entry into human respiratory epithelial cells with notable virus-specific differences.

2. Results

2.1. Pseudovirions carrying the envelope glycoproteins of HTNV and ANDV differ in entry kinetics and pH requirements leading to membrane fusion

A major challenge for work with live hantaviruses are the strict biosafety requirements limiting work to BSL3 facilities. In the past years, recombinant vesicular stomatitis virus (VSV)-derived pseudoviruses displaying heterologous viral glycoproteins were used in seminal studies to uncover entry factors for hantaviruses, filoviruses, arenaviruses, and phleboviruses (Carette et al., 2011; Jae et al., 2014, 2013; Jangra et al., 2018; Kondratowicz et al., 2011; Raaben et al., 2017; Riblett et al., 2015). The studies revealed a very close correlation of pseudotyped recombinant VSV with the authentic viruses. For our present study, we therefore generated recombinant VSV pseudoparticles bearing the glycoproteins of the prototypic Old World hantavirus HTNV and the South American ANDV. Briefly, HEK293F cell were transfected with a plasmid expressing recombinant ANDV and HTNV glycoproteins, followed by infection with recombinant VSV* ΔG-Luc in which the glycoprotein (G) gene was deleted and replaced with reporter genes encoding enhanced green fluorescent protein (EGFP; indicated by an asterisk) and firefly luciferase (Luc) (Berger Rentsch and Zimmer, 2011). VSV* ΔG-Luc was propagated on VSV-G protein-expressing cells resulting in VSV-G *trans*-complemented VSV* ΔG-Luc(VSV-G) particles. When cells expressing hantavirus glycoproteins were infected with VSV* ΔG-Luc(VSV-G), the hantavirus glycoproteins were incorporated into the viral envelope. The resulting VSV* ΔG-Luc pseudotypes were infectious and replication-competent but unable to produce infectious progeny virus making them suitable for work at BSL2. In our hands, the glycoproteins of ANDV and HTNV incorporated less efficiently into the VSV envelope compared to other viral glycoproteins, resulting in significant background due to residual VSV* ΔG-Luc(VSV-G) present in our preparations. To overcome this limitation, the pseudotypes VSV* ΔG-Luc(HTNV-G) containing HTNV-G and VSV* ΔG-Luc(ANDV-G) containing ANDV-G were produced in the presence of the potent neutralizing anti-VSVG mAb I-1 (Holland et al., 1989), resulting in virtually negligible background. This approach yielded VSV pseudoparticles at robust specific titers of 10^5–10^6 IU/ML, compatible with our needs (Fig. 1A, B). Measurement of luciferase activity and counting of EGFP expressing cells in parallel specimens revealed a good correlation between the number of EGFP-positive cells and luminescence (data not shown), allowing the use of the luciferase reporter to quantify infection in a semi-high-throughput assay format.

Upon receptor-mediated endocytosis, hantaviruses are delivered to acidified endosomal compartments (Jin et al., 2002; Ramanathan and Jonsson, 2008), where low pH induces membrane fusion (Cifuentes-Munoz et al., 2014). In a first step, we investigated the kinetics of endosomal escape of VSV* ΔG-Luc(HTNV-G) and VSV* ΔG-Luc(ANDV-G) using the well-characterized human epithelial cell line A549. Specifically, we determined the time required for the pseudotypes to become resistant to the lysosomotropic agent ammonium chloride. When added to cells, ammonium chloride rapidly depletes the endosomal pH gradient and blocks low-pH-dependent cellular processes without causing overall cytotoxicity (Rojek et al., 2008). As benchmarks, we included VSV* ΔG-Luc(VSV-G) that exit from early endosomes (Johannsdottir et al., 2009) and VSV* ΔG-Luc(LCMV-GP) pseudotypes decorated with the glycoproteins derived from the Old World arenavirus lymphocytic choriomeningitis virus (LCMV), that undergoes fusion at late endosomes (Pasqual et al., 2011). To allow virus-cell attachment without internalization, A549 cells were incubated with pseudotypes at 4 °C for 1.5 h. Unbound virus was removed, and cells rapidly shifted to 37 °C to allow internalization. After different time points, 20 mM ammonium chloride was added to cells and kept throughout the experiment to block further entry via low pH-triggered membrane fusion. The number of infected cells was determined after 16 h by counting EGFP-positive cells. Pseudotypes bearing VSV-G and LCMV-GP envelope glycoproteins escaped with a half-times of circa 10 and 45 min, respectively, as expected (Johannsdottir et al., 2009; Pasqual et al., 2011). Endosomal escape of VSV* ΔG-Luc(HTNV-G) and VSV* ΔG-Luc(ANDV-G) pseudotypes occurred with distinct half times of < 30 min and > 45 min, respectively (Fig. 1C, E), indicating different entry kinetics.

The transition from early to late endosomal compartments is accompanied by progressive acidification of the luminal space, resulting in a pH gradient that serves as guidance cue for viruses to trigger fusion (Yamauchi and Greber, 2016). To assess the pH threshold of membrane fusion by VSV* ΔG-Luc(HTNV-G) and VSV* ΔG-Luc(ANDV-G), we progressively raised the endosomal pH by adding increasing concentrations of ammonium chloride to cells and monitored productive entry. In line with the differential kinetics of endosomal escape (Fig. 1C, E), VSV* ΔG-Luc(ANDV-G) displayed higher sensitivity to ammonium chloride than VSV* ΔG-Luc(HTNV-G), indicating that the latter escapes from earlier, less acidified compartments (Fig. 1D, E). This observation is consistent with the previously reported membrane fusion by ANDV-G and HTNV-G at pH 5.9 and 6.3, respectively (Cifuentes-Munoz et al., 2011; Ogino et al., 2004). Interestingly, despite faster entry kinetics, VSV* ΔG-Luc(VSV-G) appeared more sensitive to ammonium chloride compared to VSV* ΔG-Luc(HTNV-G) (Fig. 1C, D). This suggested delayed escape of VSV* ΔG-Luc(HTNV-G) from an earlier compartment, possibly due to the use of a different pathway of endocytosis.

2.2. Identification of cellular kinases involved in HTNV-G and ANDV-G-mediated cell entry

In a first attempt to identify novel cellular factors required for hantavirus entry, we screened a library of selected, well-defined kinase inhibitors that cover major signaling pathways, implementing our pseudotypes in a semi-high-throughput assay format. To avoid artifacts due to toxicity, the candidate compounds underwent previous evaluation in a cell viability test that detects changes in cellular ATP levels under the exact assay conditions. Candidate inhibitors that resulted in $> 20\%$ reduced cell viability under the assay conditions were excluded from the screen (Fig. 2D). For positive screening, A549 cells were treated with candidate compounds for 30 min, followed by infection with VSV* ΔG-Luc(HTNV-G) (Fig. 2A) and VSV* ΔG-Luc(ANDV-G) (Fig. 2B) (MOI of 0.05) in the presence of the drugs for 1.5 h. Drugs were washed out, cells cultured in the presence of 20 mM ammonium chloride for 16 h, and productive infection detected by luciferase assay. For comparison, we included VSV* ΔG-Luc(VSV-G) (Fig. 2C). Candidate inhibitors that resulted in reproducibly $> 70\%$ reduction of pseudotype

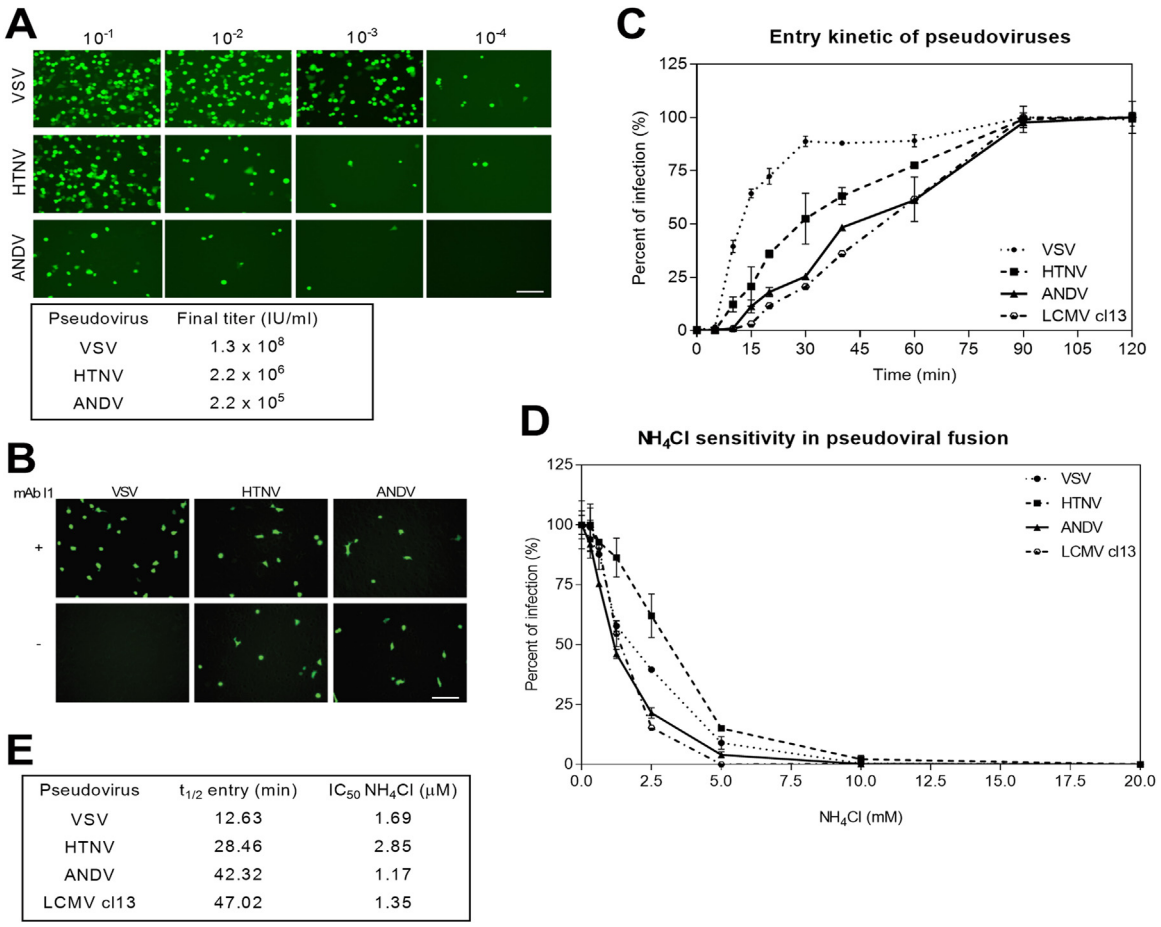

Fig. 1. Characterization of pseudotype viruses. (A) Titration of VSV* ΔG-Luc(VSV-G), VSV* ΔG-Luc(HTNV-G) and VSV* ΔG-Luc(ANDV-G) on A549 cells. Serial dilutions of the indicated viruses were incubated with monolayers of A549 cells, followed by detection of the EGFP reporter by direct immunofluorescence. Representative titers are indicated. Bar = 100 μM. (B) Specificity to neutralizing activity of anti-VSV-G antibody. A549 cells were infected with VSV* ΔG-Luc(VSV-G), VSV* ΔG-Luc(HTNV-G) and VSV* ΔG-Luc(ANDV-G) in the presence or absence of the VSVG neutralizing antibody I1 (I1 mAb). Bar = 100 μM. (C) Kinetics of endosomal escape of pseudoviruses. VSV* ΔG-Luc(VSV-G), VSV* ΔG-Luc(HTNV-G), VSV* ΔG-Luc(ANDV-G) and VSV* ΔG-Luc(LCMV-GP) (200 IU/well) were attached to monolayers of A549 cells in the cold for 1.5 h. Unbound virus was removed, and the cells rapidly shifted to 37 °C. At the indicated time points, 20 mM ammonium chloride was added and left throughout the experiment. After 16 h, infection was assessed by counting EGFP-positive cells per well. Data are means ± SD (n = 3). (D) Ammonium chloride sensitivity of viral membrane fusion. A549 cell monolayers were infected with VSV* ΔG-Luc(VSV-G), VSV* ΔG-Luc(HTNV-G), VSV* ΔG-Luc(ANDV-G) and VSV* ΔG-Luc(LCMV-GP) in presence of the indicated concentrations of ammonium chloride and incubated 1.5 h at 37 °C. After removing the inoculum, 20 mM ammonium chloride was added to block all pH-dependent viral fusion. After 16 h, productive infection was assessed by counting EGFP-positive cells per well. Data are means ± SD (n = 3). (E) Calculated $t_{1/2}$ and IC_{50} values of (B) and (C), respectively.

infection in two independent screens were considered as hits. The broadly active tyrosine kinase inhibitor tyrphostin-9 and the compound GF109203X blocked entry of all pseudotypes tested (Fig. 2A-C). Overall, the inhibition profile of VSV* ΔG-Luc(HTNV-G) resembled that of VSV* ΔG-Luc(VSV-G), with the exception of sunitinib that showed some specificity for HTNV-G (Fig. 2A, C). In contrast, comparison of the profiles obtained with VSV* ΔG-Luc(HTNV-G) and VSV* ΔG-Luc(ANDV-G) revealed significant differences including several candidate compounds that specifically inhibited VSV* ΔG-Luc(ANDV-G) but not VSV* ΔG-Luc(HTNV-G). Of particular interest were the epithelial growth factor receptor (EGFR) inhibitor gefitinib and the myosin light chain kinase (MLCK) inhibitors ML-7 and ML-9, which block entry of several viruses via macropinocytosis (Mercer and Helenius, 2009, 2012).

2.3. Entry of HTNV-G and ANDV-G pseudoviruses into epithelial cells shows hallmarks of macropinocytosis

Over the past years, macropinocytosis has emerged as a major entry pathway for a range of animal viruses (Mercer and Helenius, 2009, 2012). To further investigate a possible role of this important endocytic route in hantavirus entry, we applied a panel of well-defined "diagnostic" inhibitors against cellular factors involved in macropinocytosis proposed by Mercer and Helenius (Mercer and Helenius, 2009, 2012). To minimize duration of drug exposure and avoid unwanted off-target effects, cells were treated with the inhibitor for 30 min, followed by infection with the pseudoviruses in the presence of the inhibitor (Fig. 3A). After 1.5 h, the inhibitor was washed out with medium containing 20 mM ammonium chloride to block further entry. Productive infection was assessed after 16 h by counting EGFP-positive cells or by luciferase assay. A conserved hallmark of macropinocytosis is the dependence on sodium proton exchangers (NHE), which are sensitive to amiloride drugs such as 5-(*N*-ethyl-*N*-isopropyl)-amiloride (EIPA) (Mercer and Helenius, 2009, 2012). Entry of VSV* ΔG-Luc(HTNV-G) and VSV* ΔG-Luc(ANDV-G), but not of recombinant human adenovirus (AdV)-5, was inhibited by EIPA in a dose-dependent manner, without causing significant toxicity (Fig. 3B). In the presence of EIPA, the number of infected cells was reduced, whereas the remaining infected cells exhibited similar levels of EGFP, consistent with inhibition of viral entry (Fig. 3C). Since dependence on actin is another essential feature of macropinocytosis (Mercer and Helenius, 2009, 2012), we treated cells with cytochalasin D, which disrupts actin filaments, as well as

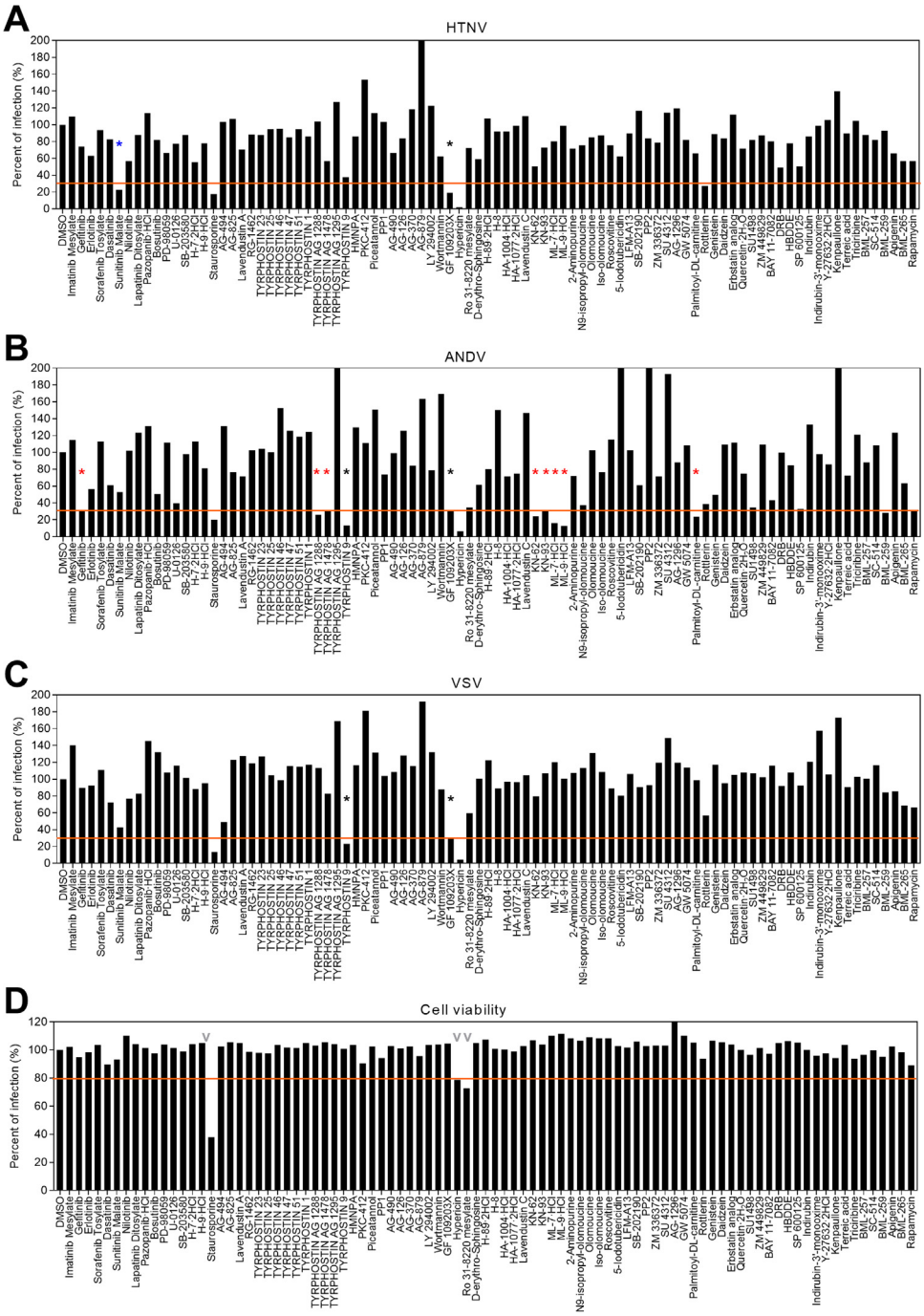

Fig. 2. Screening of kinase inhibitor library identified cellular factors implicated in viral entry. (A–C) A549 cells were pretreated with 10 μM of compounds for 30 min and infected with VSV* ΔG-Luc(HTNV-G), VSV* ΔG-Luc (ANDV-G), and VSV* ΔG-Luc(VSV-G) in the presence of drugs. After 1.5 h, cells were washed three times with medium containing 20 mM ammonium chloride, followed by 16 h of incubation in the presence of the lysosomotropic agent. Infection was detected by luciferase assay and the control (DMSO) set at 100%. Stars indicate candidate compounds that showed ≥ 70% inhibition in two independent screens. Black stars indicate broadly active compounds and red stars compounds that specifically lowered VSV* ΔG-Luc(ANDV-G) infection. Blue star: specific inhibitor of VSV* ΔG-Luc(HTNV-G). (D) Cell viability was monitored by the CellTiter-Glo® assay. The gray V symbol indicates kinase inhibitors that let to ≥ 20% reduction in cellular ATP levels and were considered toxic. Infection was detected by luciferase assay and the control (DMSO) set at 100%.

jasplakinolide, which stabilizes actin fibers. Treatment with the two inhibitors reduced subsequent infection with VSV* ΔG-Luc(HTNV-G) and VSV* ΔG-Luc(ANDV-G), without affecting cell viability (Fig. 3D). To exclude possible effects of actin inhibitors on post-entry steps of infection, we added the inhibitors after viral cell entry. In contrast to the marked reduction of viral entry, cytochalasin D and jasplakinolide did not affect post-entry steps of infection (Fig. 3E).

Macropinocytosis is constitutively active in some cell types, e.g. professional phagocytes, whereas in most cells, including epithelia, the pathway needs to be activated (Mercer and Helenius, 2012). Activation of macropinocytosis by viruses induces sometimes dramatic changes in overall cellular membrane dynamics that manifest as “blebbing” characterized by formation of dynamic membrane protrusions with concomitant cell rounding and accelerated actin depolymerization (de Vries et al., 2011; Krzyzaniak et al., 2013; Mercer and Helenius, 2008, 2009, 2012). As a first step, we investigated if engagement of A549 cells by VSV* ΔG-Luc(HTNV-G) and VSV* ΔG-Luc(ANDV-G) affects their overall morphology including the poxvirus vaccinia (VACV), which activates macropinocytosis for productive entry (Mercer and Helenius, 2008). Briefly, viruses were bound to A549 cells at high MOI (3) in the cold, unbound virus removed, and cells shifted rapidly to 37 °C. After different time points, cells were fixed and alterations in cell shape visualized by staining for filamentous (F)-actin. Consistent with previous reports (Mercer and Helenius, 2008), exposure of A549 cells to VACV induced characteristic alterations in cell shape evidenced by rounding (Fig. 4A). Exposure of cells to VSV* ΔG-Luc(HTNV-G), VSV* ΔG-Luc (ANDV-G) likewise affected cell morphology evidenced by increased cell rounding, compared to exposure to a mock preparation (Fig. 4A). Since morphological examination of cells is rather subjective, we took a more quantitative approach. Virus-induced changes in cell morphology

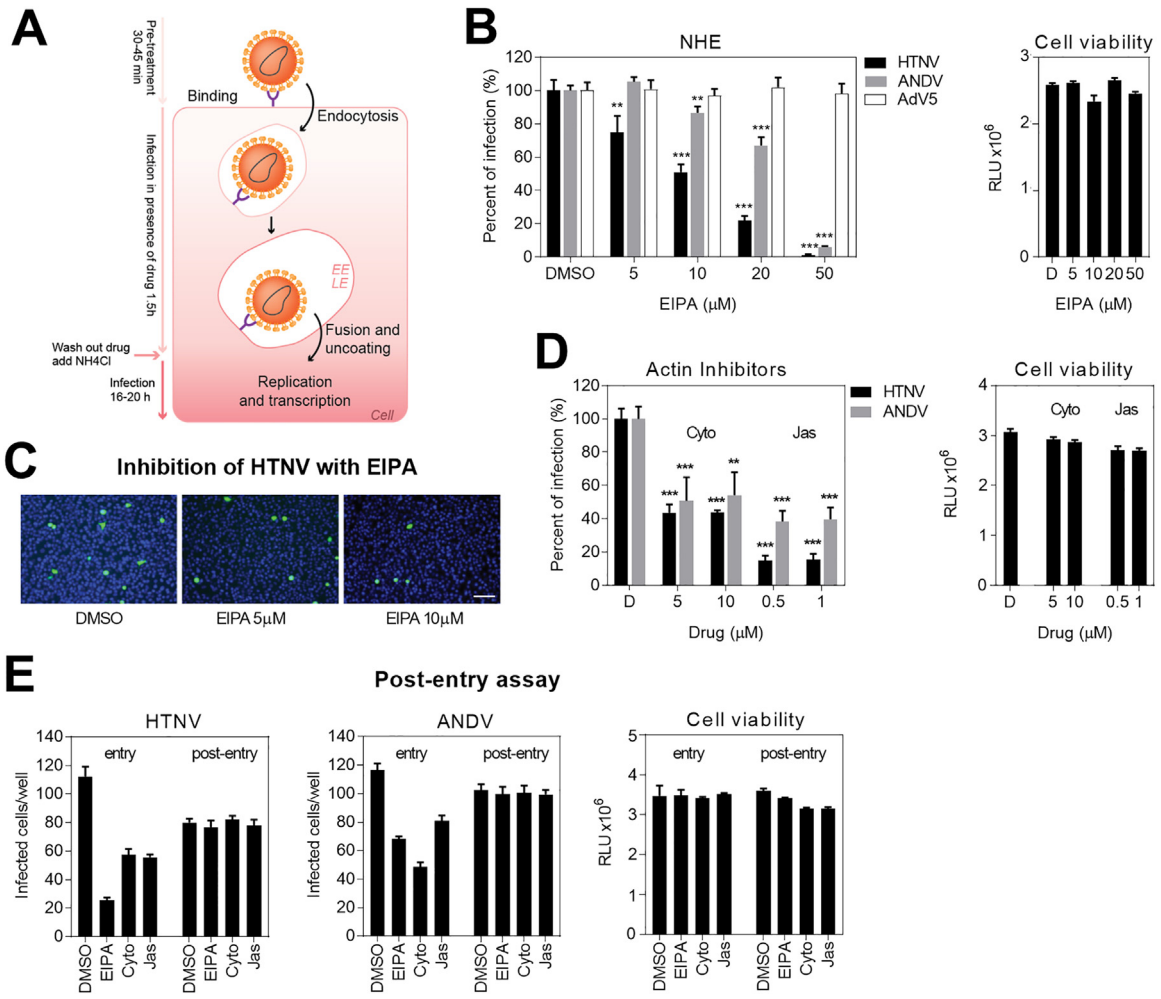

Fig. 3. Entry of VSV* ΔG-Luc(HTNV-G) and VSV* ΔG-Luc(ANDV-G) into A549 epithelial cells shows hallmarks of macropinocytosis. (A) Schema of the entry assay. For details, please see text. EE, early endosome; LE, late endosome. (B) The amiloride drug EIPA blocks entry of VSV* ΔG-Luc(HTNV-G) and VSV* ΔG-Luc(ANDV-G) without causing cell toxicity. A549 cells were treated with the indicated concentrations of EIPA for 30 min, followed by infection with VSV* ΔG-Luc(HTNV-G), VSV* ΔG-Luc(ANDV-G), and AdV5 expressing EGFP in the presence of drugs for 1.5 h. Infected cells were detected by counting EGFP-positive cells. Data are means + SD (n = 3) normalized to the DMSO control (set at 100%) and presented as percentage of infection relative to control. Data were analyzed by one-way ANOVA; *p*-value * *: $p \leq 0.01$; * **: $p \leq 0.001$. Cell toxicity was monitored by the CellTiter-Glo® assay and data represent means + SD (n = 3) of Relative Light Units (RLU). (C) Example of inhibition of VSV* ΔG-Luc(HTNV-G) by EIPA visualized by EGFP fluorescence of infected cells (B). Please note the similar EGFP fluorescence intensity with increasing EIPA concentration. Bar = 100 μm. (D) Actin inhibitors block entry of hantavirus pseudoviruses without affecting cell viability. A549 cells were pretreated with the indicated concentrations of cytochalasin D (Cyto) and jasplakinolide (Jas) for 30 min. Subsequent infection with VSV* ΔG-Luc(HTNV-G) and VSV* ΔG-Luc(ANDV-G) was performed in presence of drugs during 1.5 h. Productive infection was assessed as in (B). Data are means + SD (n = 3); *p*-value * *: $p \leq 0.01$; * **: $p \leq 0.001$. Cell toxicity was monitored by the CellTiter-Glo® assay and data are presented as means + SD (n = 3) of RLU. (E) Amiloride drug and actin inhibitor compounds are involved in VSV* ΔG-Luc(HTNV-G) and VSV* ΔG-Luc(ANDV-G) entry but not post-entry steps of infection. Effects on viral entry were assessed as described in (B) and (D), with A549 cells being treated with EIPA (20 μM), cytochalasin D (5 μM) and jasplakinolide (0.5 μM). For the post-entry assay, infection with VSV* ΔG-Luc(HTNV-G) and VSV* ΔG-Luc(ANDV-G) took place in absence of inhibitors. After removing the inoculum and washing the cells, EIPA (20 μM), cytochalasin D (5 μM) and jasplakinolide (0.5 μM) were added together with 20 mM ammonium chloride and the cells left overnight. Data are means + SD (n = 3). Cell viability was assessed by the CellTiter-Glo® assay, based on the post-entry experiment setting. Data are shown as means + SD (n = 3) of RLU.

and actin distribution that accompany viral entry via macropinocytosis often correlate with increased F-actin depolymerization (Mercer and Helenius, 2009, 2012; Mercer et al., 2010). Using a recently developed assay, we therefore quantitatively assessed the ratios of globular monomer (G)-actin vs. F-actin upon exposure of cells to VSV* ΔG-Luc (HTNV-G) and VSV* ΔG-Luc(ANDV-G), using VACV and jasplakinolide that stabilizes F-actin as positive and negative controls, respectively (Krzyzaniak et al., 2013). A549 cells were exposed to viruses at high MOI (3). At the indicated time points, cells were lysed under conditions that specifically solubilize G-actin, but not F-actin as detailed in Materials and Methods. After fractionation by micro-scale ultracentrifugation, supernatant and pellets were analyzed for actin content by Western blot. As expected, engagement of VACV resulted in marked de-polymerization of F-actin after 60 min, evidenced by an increased ratio of G/F-actin (Fig. 4B, C). VSV* ΔG-Luc(HTNV-G) and VSV* ΔG-Luc (ANDV-G) likewise shifted the equilibrium in favor of G-actin, albeit less efficiently, in particular in case of HTNV (Fig. 4B, C). In sum, the data suggested that entry of HTNV-G and ANDV-G pseudoviruses into epithelial cells shows hallmarks of macropinocytosis.

2.4. Entry of HTNV-G and ANDV-G pseudoviruses differentially depends on cellular factors involved in the regulation of macropinocytosis

In addition to NHE and actin, macropinosome formation requires several regulatory factors, including the small GTPases Cdc42 and Rac1, p21-activating kinase-1 (PAK1), neuronal Wiskott-Aldrich syndrome protein (N-WASP), phosphoinositol-3 kinase (PI3K), and the actin-related protein 2/3 (Arp2/3) (Mercer and Helenius, 2012). As a

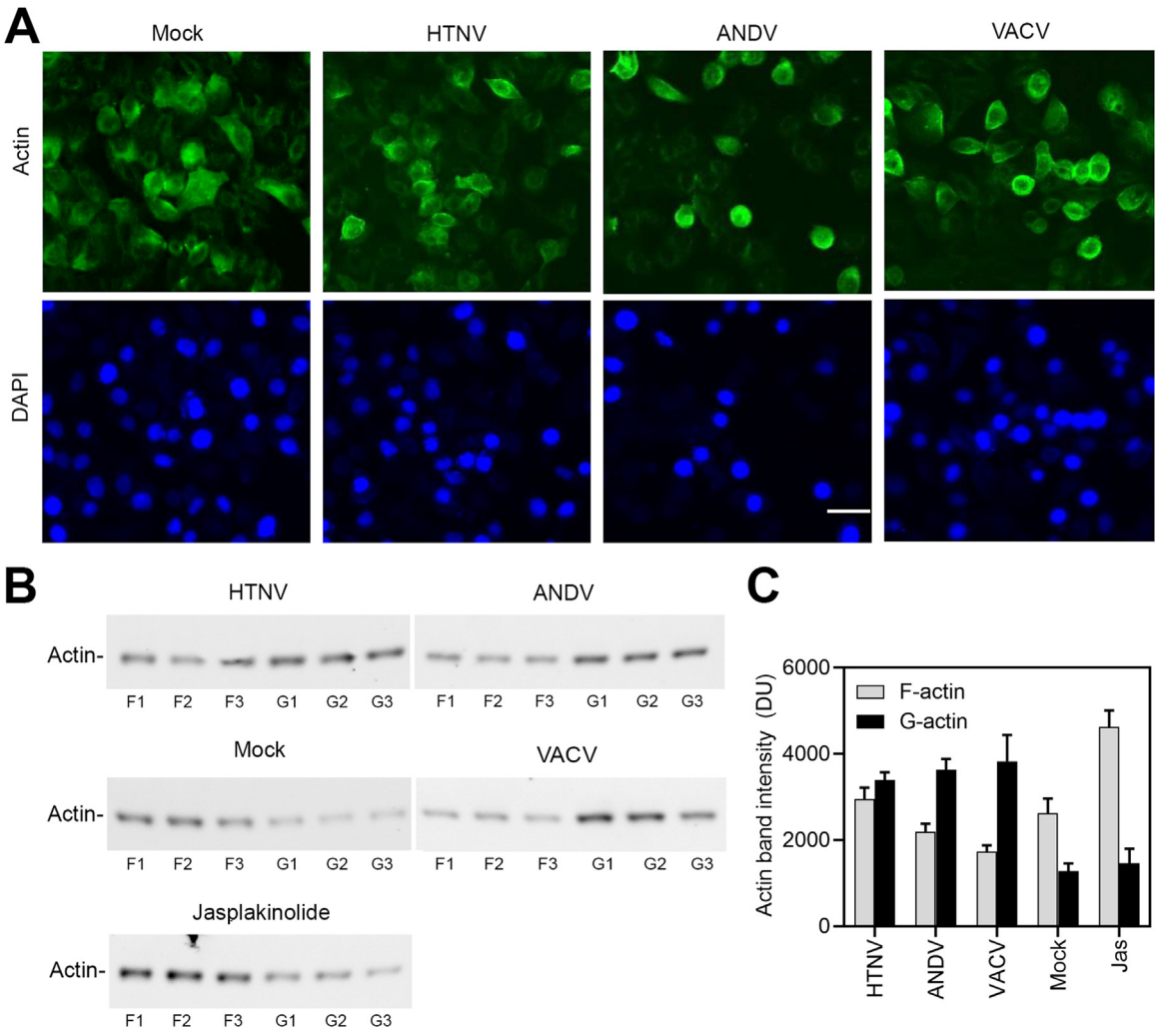

Fig. 4. Exposure of A549 cells to VSV* ΔG-Luc(HTNV-G) and VSV* ΔG-Luc(ANDV-G) changes cellular actin dynamics. (A) Changes in cell morphology induced by VSV* ΔG-Luc(HTNV-G) and VSV* ΔG-Luc(ANDV-G). Sub-confluent A549 cells were mock-treated or exposed to VSV* ΔG-Luc(HTNV-G), VSV* ΔG-Luc(ANDV-G), or VACV (3 IU/cell) for one hour in the cold. Please note that the indicated MOI of 3 IU/cell likely underestimates the number of virus particles/cell, due to a IU/particle ratio < 1 for the viruses used. Cells were shifted to 37 °C for 60 min, fixed, and F-actin staining performed with phalloidin-FITC (bar = 20 μm). (B) Quantitative assessment of changes in actin polymerization during virus entry. Triplicate specimens of A549 cells were exposed to VSV* ΔG-Luc(HTNV-G), VSV* ΔG-Luc(ANDV-G), or VACV-RFP (3 IU/cells) as in (A). As a negative control, we included 1 μM jasplakinolide. Lysis conditions specifically solubilize G-actin, but not F-actin, allowing fractionation by micro-scale ultracentrifugation. Pellets containing F-actin (F1–3) and supernatants containing G-actin (G1–3) were mixed with SDS-PAGE sample buffer and equal relative amounts probed in Western blot. Please note the shift towards more G-actin in specimens exposed to VSV* ΔG-Luc(HTNV-G), VSV* ΔG-Luc(ANDV-G), or VACV-RFP, but not mock or jasplakinolide. (C) Quantification of (B). Actin signals in the blots in (B) were quantified by densitometry. Data are means of the triplicate signals + SD in arbitrary densitometric units.

next step, we therefore addressed the role of Cdc42 and Rac1 in VSV* ΔG-Luc(HTNV-G) and VSV* ΔG-Luc(ANDV-G) entry into A549 cells using the well-known inhibitors Pirl1 and NSC 23766. Pirl1 specifically inhibited entry of VSV* ΔG-Luc(ANDV-G) but not of VSV* ΔG-Luc(HTNV-G), indicating that Cdc42 has a specific, non-redundant role in the entry of ANDV but not of HTNV (Fig. 5A). The Rac1 inhibitor NSC 23766 showed no effect on any of the pseudotypes, but reduced entry of VACV, as expected (Fig. 5B). Infection of VSV* ΔG-Luc(HTNV-G) and VSV* ΔG-Luc(ANDV-G) infection were significantly reduced after inhibition of PAK1 and N-WASP by IPA-3 and wiskostatin, respectively (Fig. 5C, E). Infection of VSV* ΔG-Luc(ANDV-G), but not VSV* ΔG-Luc(HTNV-G) was reduced after inhibition of PI3K with wortmannin (Fig. 5D). Neither VSV* ΔG-Luc(ANDV-G) nor VSV* ΔG-Luc(HTNV-G) were affected by the Arp2/3 inhibitor CK869 (Fig. 5F).

In most cell types, macropinocytosis is not constitutively active, but can be induced by activation of receptor tyrosine kinases (RTK) and other signaling receptors. In particular, the RTKs EGFR and hepatocyte growth factor (HGFR) have been linked to entry of several viruses via macropinocytosis (Eierhoff et al., 2010; Krzyzaniak et al., 2013; Mercer and Helenius, 2008; Oppliger et al., 2016). To investigate a possible role of EGFR and HGFR in VSV* ΔG-Luc(HTNV-G) and VSV* ΔG-Luc (ANDV-G) entry, we employed the inhibitors gefitinib and EMD 1214063. Gefitinib and EMD 1214063 markedly reduced the infectivity of VSV* ΔG-Luc(ANDV-G), but had only mild effects on VSV* ΔG-Luc (HTNV-G) (Fig. 6A, B). Productive entry of viruses via macropinocytosis often depends on non-muscle myosin II that is involved in fission of macropinosomes (Mercer and Helenius, 2009). In accordance with the role of macropinocytosis in the entry of hantaviruses, the MLCK inhibitors ML-7 and ML-9 were identified as hits in our screen (Fig. 2B). Examination of the dose-dependent inhibition of pseudotype entry by ML-7 showed that VSV* ΔG-Luc(ANDV-G) was highly sensitive to this drug whereas VSV* ΔG-Luc(HTNV-G) was blocked only by higher drug concentrations (Fig. 6C).

To avoid possible artifacts linked to the A549 cell line chosen for our study, we validated selected candidate inhibitors in the well-established human lung epithelial line WI-26VA4. Titration of VSV* ΔG-Luc(HTNV-

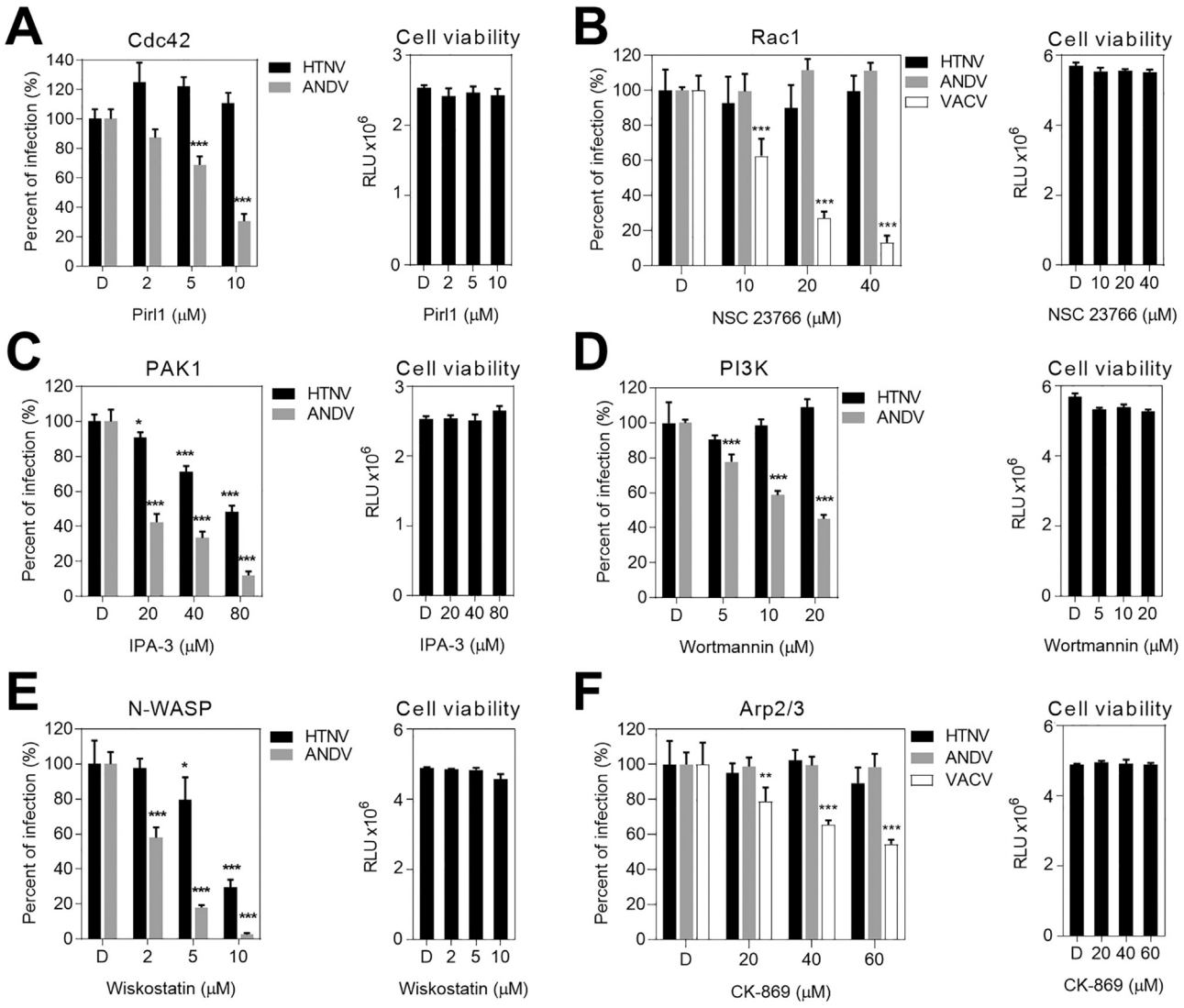

Fig. 5. VSV* ΔG-Luc(HTNV-G) and VSV* ΔG-Luc(ANDV-G) show differential dependence on cellular factors implicated in macropinocytosis. (A-F) Monolayers of A549 cells were pretreated with the indicated drugs at the given concentrations and then infected for 1.5 h with HTNV-G and ANDV-G pseudoviruses as in (3 A). VACV was included as positive control where indicated. At 16 h p.i., productive infection was detected by counting EGFP-positive cells and the DMSO (D) control set at 100%. VACV was quantified by detection of the RFP reporter by direct fluorescence, scoring red cells. Data are means + SD, (n = 3) with *p*-values * : $p \leq 0.05$; * *: $p \leq 0.01$; * **: $p \leq 0.001$. Cell viability was assessed by the CellTiter-Glo® assay. Data are shown as means + SD (n = 3) in RLU.

G) and VSV* ΔG-Luc(ANDV-G) in WI-26VA4 cells resulted in similar relative titers as in A549 cells, albeit with lower overall infectivity (Fig. 7A). As previously observed in A549 cells (Fig. 3), entry of VSV* ΔG-Luc(HTNV-G) and VSV* ΔG-Luc(ANDV-G) into WI-26VA4 cells critically depended on NHE and actin (Fig. 7B, F). Interestingly, the Cdc42 inhibitor Pirl1 that markedly reduced VSV* ΔG-Luc(ANDV-G) infection in A549 cells showed only a mild effect in WI-26VA4 cells (Fig. 7C), suggesting cell-type specific differences. Infection of both VSV* ΔG-Luc(HTNV-G) and VSV* ΔG-Luc(ANDV-G) in WI-26VA4 cells showed dependence on PAK1 and MLCK (Fig. 7D, E), as previously observed in A549 cells (Figs. 5C and 6C). The overall similarity of the inhibitor profile in two different well-established human respiratory epithelial cell lines further supports a role for macropinocytosis in HTNV and ANDV entry into this cell type.

In sum, examination of candidate cellular factors involved in macropinocytosis revealed that entry mediated by both HTNV-G and ANDV-G into human epithelial cells critically depended on NHE and actin, fulfilling the basic criteria for macropinocytosis (Mercer and Helenius, 2009, 2012). However, entry mediated by HTNV-G and ANDV-G depended on only partially overlapping sets of regulatory factors, revealing important virus-specific differences.

3. Discussion

Previous studies revealed complex cell type-specific use of different endocytic pathways by hantaviruses for cell entry (Chiang et al., 2016; Gavrilovskaya et al., 1999, 1998; Jin et al., 2002; Kleinfelter et al., 2015; Krautkramer and Zeier, 2008; Petersen et al., 2014; Popugaeva et al., 2012; Ramanathan and Jonsson, 2008; Raymond et al., 2005). To explore the largely unknown mechanisms of HTNV and ANDV entry into human respiratory epithelial cells, we combined an unbiased small molecule screen with functional studies using specific inhibitors for endocytosis. To circumvent biosafety restrictions, we employed a biocontained recombinant VSV-based pseudotype platform to perform viral entry studies. Recombinant VSV pseudoviruses have become powerful BSL2 surrogates to study cell entry of highly pathogenic emerging viruses, including hantaviruses (Brouillette et al., 2018; Carette et al., 2011; Jae et al., 2014, 2013; Jangra et al., 2018; Jemielity et al., 2013; Kondratowicz et al., 2011; Moller-Tank et al., 2014, 2013; Raaben et al., 2017; Riblett et al., 2015). Monitoring pH-dependence

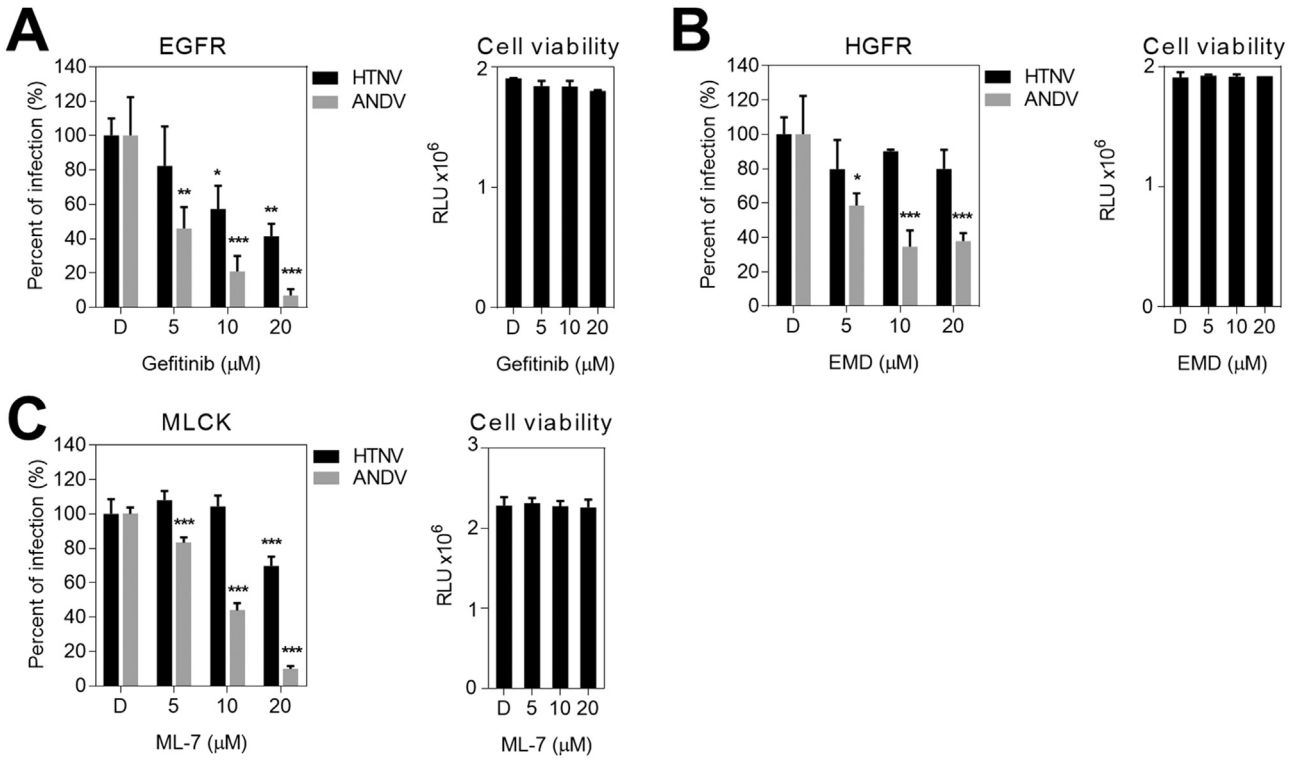

Fig. 6. Inhibitors of receptor tyrosine kinases and myosin kinase. (A-B) HTNV-G and ANDV-G pseudoviruses entry is dependent on EGFR but only ANDV-G pseudovirus entry requires HGFR. A549 cells were pretreated for 30 min with the indicated concentrations of inhibitors. Cells were then infected with VSV* ΔG-Luc (HTNV-G) and VSV* ΔG-Luc(ANDV-G) in the presence of the drug for 1.5 h. After wash-out of the drug, fresh complete medium containing 20 mM ammonium chloride was added and cells incubated at 37 °C for 1.5 h. Infection was detected by direct EGFP fluorescence and the DMSO control set at 100%. Data are means + SD (n = 3), with *p*-value * : $p \leq 0.05$; * *: $p \leq 0.01$; * * * : $p \leq 0.001$. Cell viability was determined by the CellTiter-Glo® assay. Data are means + SD, (n = 3). (C) A549 cells were treated with different concentration of ML-7 for 30 min and infected with VSV* ΔG-Luc(HTNV-G) and VSV* ΔG-Luc(ANDV-G) in the presence of the drugs. After 1.5 h, cells were washed 3 times with medium containing 20 mM ammonium chloride, followed by 16 h of incubation in the presence of the lysosomotropic agent. Infection was assessed by counting of EGFP-positive cells and the control (DMSO) set at 100%. Data are means + SD (n = 3) with *p*-value * * * : $p \leq 0.001$. Cell viability was determined by CellTiter-Glo® assay. Data are means + SD (n = 3).

and entry kinetics of VSV* ΔG-Luc(HTNV-G) and VSV* ΔG-Luc(ANDV-G), we verified the previously reported differences in the pH values required to trigger membrane fusion by these viruses (Cifuentes-Munoz et al., 2011; Ogino et al., 2004; Ray et al., 2010). As expected, the distinct membrane fusion-triggering pH values correlated with differential entry kinetics, further supporting the notion that HTNV and ANDV escape from early and late endosomal compartments, respectively.

In a first step, we used our pseudotypes to screen a kinase inhibitor library covering major signaling pathways implicated in viral entry in a semi-high-throughput assay. Our screen identified only partially overlapping sets of cellular kinases required for cell entry of VSV* ΔG-Luc (HTNV-G) and VSV* ΔG-Luc(ANDV-G), suggesting virus-specific differences. The screening data further provided first evidence of a possible link between hantavirus entry and macropinocytosis, which is increasingly recognized as a major viral entry pathway hijacked by important airborne human pathogens such as poxviruses (Mercer and Helenius, 2008), respiratory syncytial virus (RSV) (Krzyzaniak et al., 2013), and influenza A virus (de Vries et al., 2011).

For further validation, we used a “diagnostic” panel of well-defined inhibitors of regulatory factors involved in macropinocytosis. Entry of both VSV* ΔG-Luc(HTNV-G) and VSV* ΔG-Luc(ANDV-G) into A549 and WI-26VA4 human epithelial cells and critically depended on NHE and actin, which are considered as major non-redundant hallmarks of macropinocytosis (Mercer and Helenius, 2012). Inhibition of NHE by amiloride drugs lowers the sub-membrane pH and prevents activation of the small GTPases Cdc42 and Rac1 that are key regulators of actin dynamics (Koivusalo et al., 2010). Several viruses that enter via macropinocytosis such as VACV (Mercer and Helenius, 2008), RSV (Krzyzaniak et al., 2013), and African swine fever virus (Sanchez et al., 2012), show strict dependence on both Cdc42 and Rac1. Using the specific inhibitor Pirl1, we found a non-redundant role for Cdc42 in entry of VSV* ΔG-Luc(ANDV-G) into A549 cells, but not WI-26VA4 cells, suggesting cell-type specific differences. In contrast, VSV* ΔG-Luc (HTNV-G) entered both A549 and WI-26VA4 cells independently of Cdc42. None of the viruses required Rac1 for entry, suggesting redundant roles for Rac1 in entry via macropinocytosis at least for some viruses. Both, VSV* ΔG-Luc(ANDV-G) and VSV* ΔG-Luc(HTNV-G) showed dependence on PAK1 and N-WASP, whereas the Arp2/3 complex seemed dispensable for entry. Monitoring dose-dependence of inhibition revealed higher dependence of VSV* ΔG-Luc(ANDV-G) on PAK1 and N-WASP compared to VSV* ΔG-Luc(HTNV-G). The reasons for this phenomenon are currently unclear and may relate to different roles of upstream regulatory factors.

Macropinocytosis is constitutively active in specialized cell types, whereas in most cells, including epithelial cells, the pathway needs to be activated via signaling receptors like RTKs and integrins. Our studies identified EGFR and HGFR as previously unknown entry factors for hantavirus cell entry. Both RTK are widely expressed in different human epithelial cells types and can contribute to viral entry via macropinocytosis (Eierhoff et al., 2010; Krzyzaniak et al., 2013; Mercer and Helenius, 2008; Oppliger et al., 2016). Inhibition of EGFR reduced entry of VSV* ΔG-Luc(ANDV-G) and VSV* ΔG-Luc(HTNV-G), whereas blocking of HGFR selectively affected VSV* ΔG-Luc(ANDV-G) entry. Together with the differential requirement for Cdc42, these findings suggest important virus-specific differences in upstream signaling

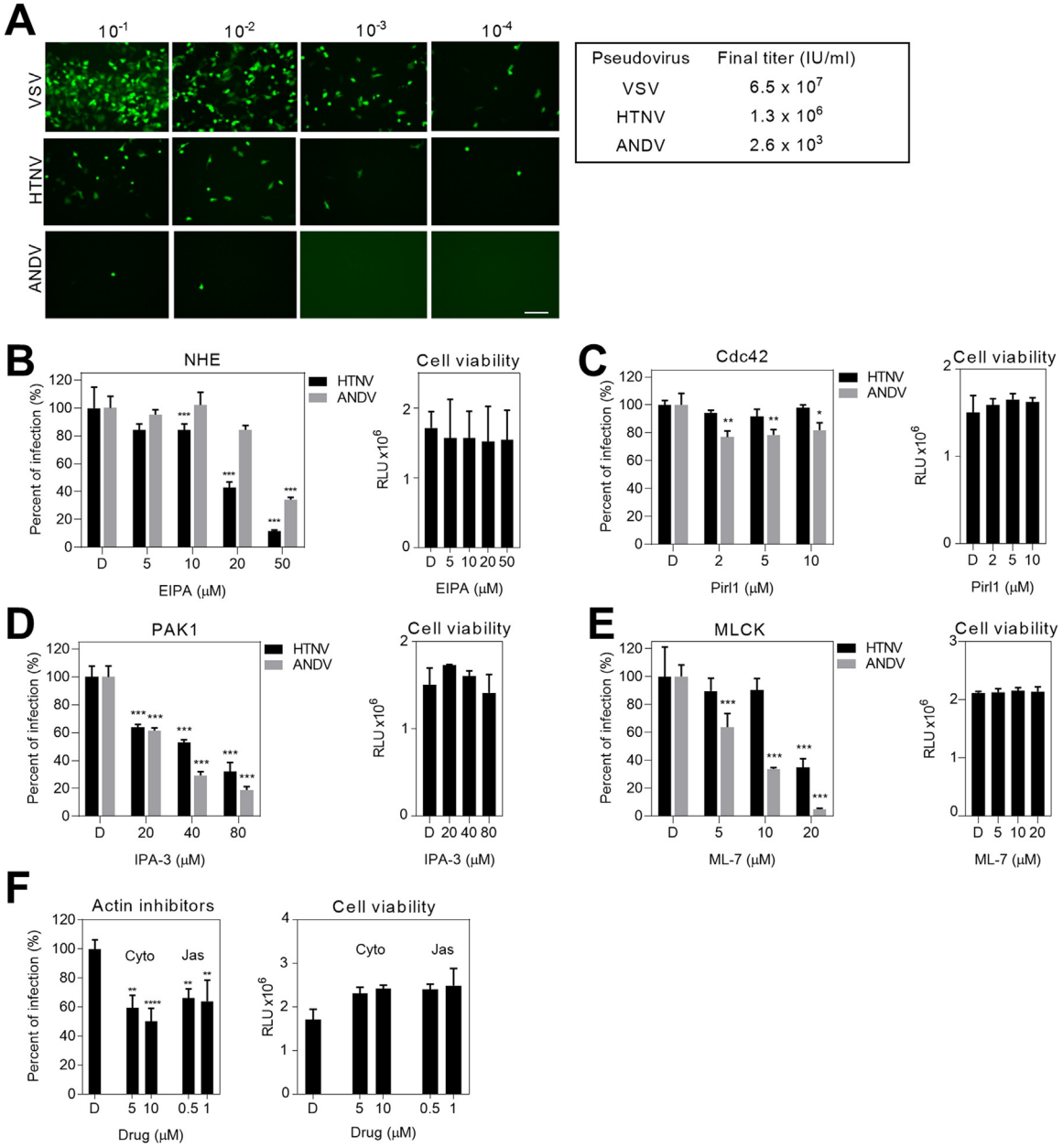

Fig. 7. Validation of selected inhibitors in the human lung epithelial cell line WI-26VA4. (A) Titration of VSV* ΔG-Luc(VSV-G), VSV* ΔG-Luc(HTNV-G) and VSV* ΔG-Luc(ANDV-G) on WI-26VA4 cells. Serial dilutions of the indicated viruses were incubated with fresh monolayers of WI-26VA4 cells, followed by detection of the EGFP reporter by direct fluorescence. Representative titers are indicated. (B-F) Monolayers of WI-26VA4 cells were pretreated with the indicated drugs at the given concentrations and then infected for 1.5 h with HTNV-G and ANDV-G pseudoviruses as in (3 A). After 16 h, productive infection was detected by counting EGPF-positive infected cells and the DMSO (D) control set at 100%. Data are means + SD, (n = 3) with p-value *: $p \leq 0.05$; **: $p \leq 0.01$; ***: $p \leq 0.001$. Cell viability was assessed by the CellTiter-Glo® assay. Data are shown as means + SD (n = 3) of Relative Light Units (RLU).

linked to uptake of VSV* ΔG-Luc(ANDV-G) and VSV* ΔG-Luc(HTNV-G). It is currently unclear if the viruses activate RTKs to promote uptake or if they depend on steady-state levels of RTK activation that serve as "permissive" signals. Notably, the EC_{50} values for RTK inhibitors gefitinib and EMD 1214063 against viral entry observed in our study were well above the EC_{50} reported for inhibition of receptor phosphorylation (Bladt et al., 2013) and we cannot formally exclude the involvement of additional, yet unknown kinases. Another notable difference was the higher sensitivity of VSV* ΔG-Luc(ANDV-G) but not VSV* ΔG-Luc (HTNV-G) towards inhibitors of myosin light chain kinase involved in closure of large macropinocytotic vesicles (Mercer and Helenius, 2012). The conserved essential roles of PAK1, N-WASP, and EGFR for VSV* ΔG-Luc(ANDV-G) and VSV* ΔG-Luc(HTNV-G) entry makes these regulatory factors possible targets for therapeutic anti-viral intervention. In a next step, we will validate selected candidate inhibitors of HTNV and ANDV entry identified here with live virus isolates under BSL3.

Previous examination of cellular factors involved in viral cell entry via macropinocytosis revealed significant variation between different viruses (Mercer and Helenius, 2009, 2012), suggesting that the pathogens can recruit specific sets of regulatory factors, according to their needs. The observed dependence of VSV* ΔG-Luc(ANDV-G) and VSV* ΔG-Luc(HTNV-G) entry on specific non-overlapping sets of known cellular regulators of macropinocytosis further supports this notion. The recently discovered differential use of PCDH1 for entry of ANDV, but not HTNV into endothelial cells (Jangra et al., 2018) opens the

possibility that HTNV-G and ANDV-G may have evolved to recognize distinct sets of receptors and/or co-receptors on human epithelial cells. Interestingly, PCDH1 is expressed in human respiratory epithelial cells (Koning et al., 2012), where it plays a role in regulation of the epithelial barrier function (Kozu et al., 2015). The exact function of PCDH1 in hantavirus entry into respiratory epithelial cells and a possible link to macropinocytosis are under investigation in our laboratory. In sum, our study defines sets of candidate cellular factors involved in HTNV and ANDV entry into a human respiratory epithelial cell line and identifies specific small molecule inhibitors. Our results may therefore help to develop urgently needed novel antiviral strategies against these emerging pathogens.

4. Materials and methods

4.1. Plasmids, antibodies, and reagents

pWRG/HTNV-M (Hooper et al., 2001) was kindly provided by Connie. S. Schmaljohn (U.S. Army Medical Research Institute of Infectious Diseases, Fort Detrick, USA). The expression plasmid pI18 for the glycoprotein of ANDV strain CHI-7913 was kindly provided by Nicole Tischler (Molecular Virology Laboratory, Fundación Ciencia & Vida, Santiago, Chile) and has been described previously (Cifuentes-Munoz et al., 2010). Expression plasmids encoding VSV-G and LCMV-GP (clone 13) have been reported previously (Perez et al., 2003). The VSV neutralizing antibody I1 (I1 mAb) has been described (Holland et al., 1989). The inhibitors included Pirl1 (Chembridge); wiskostatin (Enzo); and 5-(*N*-ethyl-*N*-isopropyl) amiloride (EIPA), NSC237766, wortmannin, cytochalasin D, IPA-3, jasplakinolide, ML-7, and ammonium chloride (NH_4Cl) (Sigma). EMD 1214063 was from Selleckchem. The SCREEN WELL® kinase inhibitor library was from Enzo Life Science (catalog no. BML-2832–0100) supplemented with a customized library containing 10 FDA-approved kinase inhibitors (imatinib mesylate, gefitinib, erlotinib, sorafenib tosylate, desatinib, sunitinib malate, nilotinib, lapatinib ditosylate, pazopanib-HCL, and bosutinib). For screening, the compounds were used at 10 μM. The CellTiter-Glo® Assay System and the ONE-Glo™ Luciferase Assay System were obtained from Promega (Madison WI).

4.2. Cells

Human lung carcinoma alveolar epithelial (A549) cells and human lung epithelial cell line WI-26VA4, were cultured in Dulbecco modified Eagle medium (DMEM) GlutaMAX™ (Gibco) supplemented with 10% (vol/vol) fetal calf serum (FCS) (Amimed) at 37 °C under 5% CO_2 atmosphere. For infection studies, 35´000 cells/ well were seeded in a 96-well plate and cultured overnight until cell monolayer formation.

4.3. Pseudotype virus production and viruses

The pseudotype viral system was based on the recombinant VSV* ΔG-Luc vector in which the glycoprotein gene (G) had been deleted and replaced with genes encoding green fluorescent protein (EGFP; indicated by an asterisk) and luciferase (Luc) (Berger Rentsch and Zimmer, 2011). HEK293F cells were plated in 10 cm dishes at 6×10^6 cells/dish and transiently transfected with plasmids encoding glycoproteins of interest using lipofectamine. After 42 h cells were transduced with VSV* ΔG-Luc(VSV-G), pseudoviruses bearing VSV-G, with an MOI = 3–5 for 2 h at 37 °C. The inoculum was removed and cells were subsequently washed twice with serum-free DMEM and incubated with fresh DMEM containing 10% FCS with an neutralizing anti-VSVG mAb I-1 diluted 1:100 in order to lower unspecific background. Twenty-four hours later, supernatants were collected and titrated. Recombinant human adenovirus serotype 5 (AdV5) expressing EGFP has been described previously (Oppliger et al., 2016). Recombinant vaccinia virus (VACV) MR strain expressing RFP (Mercer and Helenius, 2008) was provided by Jason Mercer (University College London, UK) and was produced as mature virus (Mercer and Helenius, 2008).

4.4. Entry kinetics of pseudoviruses

Confluent monolayers of A549 cells seeded in a 96-well plate were incubated on ice for 30 min. Viruses diluted in DMEM 10% (vol/vol) FCS were added to the cells and incubated in the cold for 1.5 h. After removing the inoculum, cells were washed twice with cold PBS and shifted at 37 °C by adding pre-warmed DMEM containing 10% FCS and putting the plate rapidly in the incubator at 37 °C. Ammonium chloride diluted in DMEM with 10% (vol/vol) FCS at a final concentration of 20 mM was added to the cells at the indicated time points. After 16 h of incubation at 37 °C and 5% CO_2, productive infection was quantified by counting the EGFP-positive cells per well.

4.5. Ammonium chloride sensitivity of viral glycoprotein-mediated membrane fusion

VSV* ΔG-Luc(VSV-G), VSV* ΔG-Luc(HTNV-G), VSV* ΔG-Luc(ANDV-G) and VSV* ΔG-Luc(LCMV-GP) were diluted in DMEM with 10% (vol/vol) FCS in the presence of the indicated concentration of ammonium chloride and added to A549 monolayers. After 1.5 h of incubation at 37 °C and 5% (vol/vol) CO_2, the inoculum was removed and fresh DMEM supplemented with 10% (vol/vol) FCS and 20 mM of ammonium chloride was added to the cells. After 16 h of incubation at 37 °C and 5% (vol/vol) CO_2, productive infection was quantified by counting the EGFP-positive cells per well.

4.6. Screening of a kinase inhibitor library

A549 cells were plated in each well of a 96-well plate and cultured overnight, resulting in monolayers. The cells were pretreated with candidate compounds dissolved in DMSO for 30 min. Around 4000 IU/well of VSV* ΔG-Luc(VSV-G), VSV* ΔG-Luc(HTNV-G), and VSV* ΔG-Luc(ANDV-G) were added in the presence of candidate compounds. After 1.5 h, the inoculum was removed and the cells were washed three times and incubated for 16 h in complete medium containing 20 mM ammonium chloride. Infection was quantified by measuring luciferase activity using ONE-Glo™ luciferase system. The cytotoxicity of compounds was assessed using a CellTiter-Glo® luminescent cell viability assay (Promega), which determines the number of viable cells on the basis of ATP levels. Luminescence signals were quantified by using GloMax® Multi Detection System (Promega). Kinase inhibitors that showed ≥ 70% viral inhibition were considered hits. Compounds that caused ≥ 20% reduction in cellular ATP levels according to CellTiter-Glo® assay were removed from the screen.

4.7. HTNV-G and ANDV-G pseudovirus entry assays

Cells were seeded in 96-well plates at 3.5×10^4 cells per well and grown into confluent monolayers for 16–20 h, unless stated otherwise. Cells were treated with drugs for 30 min, followed by infection with the indicated viruses in presence of the drug for 1.5 h at 37 °C. Unbound virus was removed, cells washed twice with DMEM supplemented with 20 mM ammonium chloride, and fresh complete medium added in presence of the lysosomotropic agent. At 16–20 h post-infection, productive infection was detected via the EGFP reporter using direct fluorescence using an EVOS FLoid Cell Imaging Station (ThermoFisher) or luciferase assay. Luciferase signals were detected with the ONE-Glo™ Luciferase Assay System (Promega) and a Berthold microplate fluorescence reader.

To assess possible effects of candidate inhibitors on post-entry steps, monolayers of A549 cells in a 96-well plate were infected in absence of drug with the indicated viruses for 1.5 h. The inoculum was removed

and fresh medium supplemented with the indicated candidate drugs or solvent control (DMSO) together with 20 mM ammonium chloride was added and left overnight. Productive infection was assessed 16 h post-infection by counting the EGFP-positive cells.

4.8. Quantification of filamentous (F) and globular (G) actin

Extraction of F/G actin was performed using the F/G in vitro assay kit from Cytoskeleton Inc. (BK037) following the manufacturer's instructions. Briefly, 10^5 A549 cells were seeded in 24-well plates and cultured for 24 h resulting in closed monolayers. VSV* ΔG-Luc(HTNV-G), VSV* ΔG-Luc(ANDV-G), and VACV-RFP (3 IU/cell) were added for the indicated time point at 37 °C. The indicated MOI of 3 IU/cell likely underestimates the number of virus particles, due to a IU/particle ratio < 1 for the viruses used. After brief washing in complete DMEM (pre-warmed), all liquid was removed and 100 µl of LAS2 buffer (prepared according to the manufacturers information) added per well. Cells were removed using a cell scraper and lysed for 10 min. Lysates were transferred into new tubes and subjected to low speed centrifugation (5′000 rpm for 5 min) to remove cell debris. Cleared supernatants were subjected to ultracentrifugation (100′000 g, 1 h). Pellets containing F-actin and supernatants with G-actin were suspended in equal volumes of SDS-PAGE sample buffer. Actin contents in the F- and G-actin fractions were assessed by Western blotting using anti-actin antibody contained in the kit. Signals were quantified by densitometry as described (Kunz et al., 2003).

4.9. Statistical analysis

Graphical representation and statistical analysis were performed using GraphPad Prism 7 software. P values of < 0.05 were considered statistically significant.

Acknowledgements

The authors thank Nicole Tischler (Molecular Virology Laboratory, Fundación Ciencia & Vida, Santiago, Chile) for the expression plasmid pI18 GPC ANDV and her helpful comments on the manuscript. We further thank Connie Schmaljohn (USAMRIID, Fort Detrick, MD, USA) for the plasmid pWRG/HTNV-M and Jason Mercer (University College London, UK) for the recombinant VACV expressing RFP. This research was supported by Swiss Federal Office for Civil Protection (Grant Nr. 353006233/Stm to O.E. and S.K.), Swiss Lung Association (Grant Nr.: 2016-06_Kunz to SK, OE and SR). S.K was further supported by Swiss National Science Foundation grants 310030_149746, 310030_170108, and SINERGIA Nr. CRSII3_160780/1, as well as funds by the University of Lausanne.

References

Albornoz, A., Hoffmann, A.B., Lozach, P.Y., Tischler, N.D., 2016. Early Bunyavirus-host cell interactions. Viruses 8.

Berger Rentsch, M., Zimmer, G., 2011. A vesicular stomatitis virus replicon-based bioassay for the rapid and sensitive determination of multi-species type I interferon. PLoS One 6, e25858.

Bladt, F., Faden, B., Friese-Hamim, M., Knuehl, C., Wilm, C., Fittschen, C., Gradler, U., Meyring, M., Dorsch, D., Jaehrling, F., Pehl, U., Stieber, F., Schadt, O., Blaukat, A., 2013. EMD 1214063 and EMD 1204831 constitute a new class of potent and highly selective c-Met inhibitors. Clin. Cancer Res.: Off. J. Am. Assoc. Cancer Res. 19, 2941–2951.

Brouillette, R.B., Phillips, E.K., Patel, R., Mahauad-Fernandez, W., Moller-Tank, S., Rogers, K.J., Dillard, J.A., Cooney, A.L., Martinez-Sobrido, L., Okeoma, C., Maury, W., 2018. TIM-1 mediates dystroglycan-independent entry of Lassa virus. J. Virol.

Carette, J.E., Raaben, M., Wong, A.C., Herbert, A.S., Obernosterer, G., Mulherkar, N., Kuehne, A.I., Kranzusch, P.J., Griffin, A.M., Ruthel, G., Dal Cin, P., Dye, J.M., Whelan, S.P., Chandran, K., Brummelkamp, T.R., 2011. Ebola virus entry requires the cholesterol transporter Niemann-Pick C1. Nature 477, 340–343.

Chiang, C.F., Flint, M., Lin, J.S., Spiropoulou, C.F., 2016. Endocytic pathways used by andes virus to enter primary human lung endothelial cells. PLoS One 11, e0164768.

Cifuentes-Munoz, N., Darlix, J.L., Tischler, N.D., 2010. Development of a lentiviral vector system to study the role of the Andes virus glycoproteins. Virus Res. 153, 29–35.

Cifuentes-Munoz, N., Barriga, G.P., Valenzuela, P.D., Tischler, N.D., 2011. Aromatic and polar residues spanning the candidate fusion peptide of the Andes virus Gc protein are essential for membrane fusion and infection. J. Gen. Virol. 92, 552–563.

Cifuentes-Munoz, N., Salazar-Quiroz, N., Tischler, N.D., 2014. Hantavirus Gn and Gc envelope glycoproteins: key structural units for virus cell entry and virus assembly. Viruses 6, 1801–1822.

Eierhoff, T., Hrincius, E.R., Rescher, U., Ludwig, S., Ehrhardt, C., 2010. The epidermal growth factor receptor (EGFR) promotes uptake of influenza A viruses (IAV) into host cells. PLoS Pathog. 6, e1001099.

Gavrilovskaya, I.N., Shepley, M., Shaw, R., Ginsberg, M.H., Mackow, E.R., 1998. Beta3 integrins mediate the cellular entry of hantaviruses that cause respiratory failure. Proc. Natl. Acad. Sci. USA 95, 7074–7079.

Gavrilovskaya, I.N., Brown, E.J., Ginsberg, M.H., Mackow, E.R., 1999. Cellular entry of hantaviruses which cause hemorrhagic fever with renal syndrome is mediated by beta3 integrins. J. Virol. 73, 3951–3959.

Hansen, C.G., Nichols, B.J., 2009. Molecular mechanisms of clathrin-independent endocytosis. J. Cell Sci. 122, 1713–1721.

Holland, J.J., de la Torre, J.C., Steinhauer, D.A., Clarke, D., Duarte, E., Domingo, E., 1989. Virus mutation frequencies can be greatly underestimated by monoclonal antibody neutralization of virions. J. Virol. 63, 5030–5036.

Hooper, J.W., Custer, D.M., Thompson, E., Schmaljohn, C.S., 2001. DNA vaccination with the Hantaan virus M gene protects Hamsters against three of four HFRS hantaviruses and elicits a high-titer neutralizing antibody response in Rhesus monkeys. J. Virol. 75, 8469–8477.

Jae, L.T., Raaben, M., Riemersma, M., van Beusekom, E., Blomen, V.A., Velds, A., Kerkhoven, R.M., Carette, J.E., Topaloglu, H., Meinecke, P., Wessels, M.W., Lefeber, D.J., Whelan, S.P., van Bokhoven, H., Brummelkamp, T.R., 2013. Deciphering the glycosylome of dystroglycanopathies using haploid screens for lassa virus entry. Science 340, 479–483.

Jae, L.T., Raaben, M., Herbert, A.S., Kuehne, A.I., Wirchnianski, A.S., Soh, T.K., Stubbs, S.H., Janssen, H., Damme, M., Saftig, P., Whelan, S.P., Dye, J.M., Brummelkamp, T.R., 2014. Virus entry. Lassa virus entry requires a trigger-induced receptor switch. Science 344, 1506–1510.

Jangra, R.K., Herbert, A.S., Li, R., Jae, L.T., Kleinfelter, L.M., Slough, M.M., Barker, S.L., Guardado-Calvo, P., Roman-Sosa, G., Dieterle, M.E., Kuehne, A.I., Muena, N.A., Wirchnianski, A.S., Nyakatura, E.K., Fels, J.M., Ng, M., Mittler, E., Pan, J., Bharrhan, S., Wec, A.Z., Lai, J.R., Sidhu, S.S., Tischler, N.D., Rey, F.A., Moffat, J., Brummelkamp, T.R., Wang, Z., Dye, J.M., Chandran, K., 2018. Protocadherin-1 is essential for cell entry by New World hantaviruses. Nature 563, 559–563.

Jemielity, S., Wang, J.J., Chan, Y.K., Ahmed, A.A., Li, W., Monahan, S., Bu, X., Farzan, M., Freeman, G.J., Umetsu, D.T., Dekruyff, R.H., Choe, H., 2013. TIM-family proteins promote infection of multiple enveloped viruses through virion-associated phosphatidylserine. PLoS Pathog. 9, e1003232.

Jin, M., Park, J., Lee, S., Park, B., Shin, J., Song, K.J., Ahn, T.I., Hwang, S.Y., Ahn, B.Y., Ahn, K., 2002. Hantaan virus enters cells by clathrin-dependent receptor-mediated endocytosis. Virology 294, 60–69.

Johannsdottir, H.K., Mancini, R., Kartenbeck, J., Amato, L., Helenius, A., 2009. Host cell factors and functions involved in vesicular stomatitis virus entry. J. Virol. 83, 440–453.

Jonsson, C.B., Figueiredo, L.T., Vapalahti, O., 2010. A global perspective on hantavirus ecology, epidemiology, and disease. Clin. Microbiol. Rev. 23, 412–441.

Kleinfelter, L.M., Jangra, R.K., Jae, L.T., Herbert, A.S., Mittler, E., Stiles, K.M., Wirchnianski, A.S., Kielian, M., Brummelkamp, T.R., Dye, J.M., Chandran, K., 2015. Haploid genetic screen reveals a profound and direct dependence on cholesterol for hantavirus membrane fusion. MBio 6, e00801.

Koivusalo, M., Welch, C., Hayashi, H., Scott, C.C., Kim, M., Alexander, T., Touret, N., Hahn, K.M., Grinstein, S., 2010. Amiloride inhibits macropinocytosis by lowering submembranous pH and preventing Rac1 and Cdc42 signaling. J. Cell Biol. 188, 547–563.

Kondratowicz, A.S., Lennemann, N.J., Sinn, P.L., Davey, R.A., Hunt, C.L., Moller-Tank, S., Meyerholz, D.K., Rennert, P., Mullins, R.F., Brindley, M., Sandersfeld, L.M., Quinn, K., Weller, M., McCray Jr., P.B., Chiorini, J., Maury, W., 2011. T-cell immunoglobulin and mucin domain 1 (TIM-1) is a receptor for Zaire Ebolavirus and Lake Victoria Marburgvirus. Proc. Natl. Acad. Sci. USA 108, 8426–8431.

Koning, H., Sayers, I., Stewart, C.E., de Jong, D., Ten Hacken, N.H., Postma, D.S., van Oosterhout, A.J., Nawijn, M.C., Koppelman, G.H., 2012. Characterization of protocadherin-1 expression in primary bronchial epithelial cells: association with epithelial cell differentiation. FASEB J. 26, 439–448.

Kozu, Y., Gon, Y., Maruoka, S., Kazumichi, K., Sekiyama, A., Kishi, H., Nomura, Y., Ikeda, M., Hashimoto, S., 2015. Protocadherin-1 is a glucocorticoid-responsive critical regulator of airway epithelial barrier function. BMC Pulm. Med. 15, 80.

Krautkramer, E., Zeier, M., 2008. Hantavirus causing hemorrhagic fever with renal syndrome enters from the apical surface and requires decay-accelerating factor (DAF/CD55). J. Virol. 82, 4257–4264.

Krautkramer, E., Zeier, M., 2014. Old World hantaviruses: aspects of pathogenesis and clinical course of acute renal failure. Virus Res. 187, 59–64.

Krautkramer, E., Zeier, M., Plyusnin, A., 2013. Hantavirus infection: an emerging infectious disease causing acute renal failure. Kidney Int. 83, 23–27.

Krzyzaniak, M.A., Zumstein, M.T., Gerez, J.A., Picotti, P., Helenius, A., 2013. Host cell entry of respiratory syncytial virus involves macropinocytosis followed by proteolytic activation of the F protein. PLoS Pathog. 9, e1003309.

Kunz, S., Edelmann, K.H., de la Torre, J.-C., Gorney, R., Oldstone, M.B.A., 2003. Mechanisms for lymphocytic choriomeningitis virus glycoprotein cleavage, transport, and incorporation into virions. Virology 314, 168–178.

Manigold, T., Vial, P., 2014. Human hantavirus infections: epidemiology, clinical

features, pathogenesis and immunology. Swiss Med. Wkly. 144, w13937.
Mercer, J., Helenius, A., 2008. Vaccinia virus uses macropinocytosis and apoptotic mimicry to enter host cells. Science 320, 531–535.
Mercer, J., Helenius, A., 2009. Virus entry by macropinocytosis. Nat. Cell Biol. 11, 510–520.
Mercer, J., Helenius, A., 2012. Gulping rather than sipping: macropinocytosis as a way of virus entry. Curr. Opin. Microbiol. 15, 490–499.
Mercer, J., Schelhaas, M., Helenius, A., 2010. Virus entry by endocytosis. Annu. Rev. Biochem. 79, 803–833.
Moller-Tank, S., Kondratowicz, A.S., Davey, R.A., Rennert, P.D., Maury, W., 2013. Role of the phosphatidylserine receptor TIM-1 in enveloped-virus entry. J. Virol. 87, 8327–8341.
Moller-Tank, S., Albritton, L.M., Rennert, P.D., Maury, W., 2014. Characterizing functional domains for TIM-mediated enveloped virus entry. J. Virol. 88, 6702–6713.
Muranyi, W., Bahr, U., Zeier, M., van der Woude, F.J., 2005. Hantavirus infection. J. Am. Soc. Nephrol.: JASN 16, 3669–3679.
Ogino, M., Yoshimatsu, K., Ebihara, H., Araki, K., Lee, B.H., Okumura, M., Arikawa, J., 2004. Cell fusion activities of Hantaan virus envelope glycoproteins. J. Virol. 78, 10776–10782.
Oppliger, J., Torriani, G., Herrador, A., Kunz, S., 2016. Lassa virus cell entry via dystroglycan involves an unusual pathway of macropinocytosis. J. Virol. 90, 6412–6429.
Pasqual, G., Rojek, J.M., Masin, M., Chatton, J.Y., Kunz, S., 2011. Old world arenaviruses enter the host cell via the multivesicular body and depend on the endosomal sorting complex required for transport. PLoS Pathog. 7, e1002232.
Perez, M., Craven, R.C., de la Torre, J.C., 2003. The small RING finger protein Z drives arenavirus budding: implications for antiviral strategies. Proc. Natl. Acad. Sci. USA 100, 12978–12983.
Petersen, J., Drake, M.J., Bruce, E.A., Riblett, A.M., Didigu, C.A., Wilen, C.B., Malani, N., Male, F., Lee, F.H., Bushman, F.D., Cherry, S., Doms, R.W., Bates, P., Briley Jr., K., 2014. The major cellular sterol regulatory pathway is required for Andes virus infection. PLoS Pathog. 10, e1003911.
Popugaeva, E., Witkowski, P.T., Schlegel, M., Ulrich, R.G., Auste, B., Rang, A., Kruger, D.H., Klempa, B., 2012. Dobrava-Belgrade hantavirus from Germany shows receptor usage and innate immunity induction consistent with the pathogenicity of the virus in humans. PLoS One 7, e35587.
Raaben, M., Jae, L.T., Herbert, A.S., Kuehne, A.I., Stubbs, S.H., Chou, Y.Y., Blomen, V.A., Kirchhausen, T., Dye, J.M., Brummelkamp, T.R., Whelan, S.P., 2017. NRP2 and CD63 Are Host Factors for Lujo Virus Cell Entry. Cell Host Microbe 22 (688–696), e685.
Ramanathan, H.N., Jonsson, C.B., 2008. New and old world hantaviruses differentially utilize host cytoskeletal components during their life cycles. Virology 374, 138–150.
Ray, N., Whidby, J., Stewart, S., Hooper, J.W., Bertolotti-Ciarlet, A., 2010. Study of Andes virus entry and neutralization using a pseudovirion system. J. Virol. Methods 163, 416–423.
Raymond, T., Gorbunova, E., Gavrilovskaya, I.N., Mackow, E.R., 2005. Pathogenic hantaviruses bind plexin-semaphorin-integrin domains present at the apex of inactive, bent alphavbeta3 integrin conformers. Proc. Natl. Acad. Sci. USA 102, 1163–1168.
Riblett, A.M., Blomen, V.A., Jae, L.T., Altamura, L.A., Doms, R.W., Brummelkamp, T.R., Wojcechowskyj, J.A., 2015. A haploid genetic screen identifies heparan sulfate proteoglycans supporting rift valley fever virus infection. J. Virol. 90, 1414–1423.
Rojek, J.M., Sanchez, A.B., Nguyen, N.T., de la Torre, J.C., Kunz, S., 2008. Different mechanisms of cell entry by human-pathogenic old world and new world arena viruses. J. Virol. 82, 7677–7687.
Sanchez, E.G., Quintas, A., Perez-Nunez, D., Nogal, M., Barroso, S., Carrascosa, A.L., Revilla, Y., 2012. African swine fever virus uses macropinocytosis to enter host cells. PLoS Pathog. 8, e1002754.
Tischler, N.D., Galeno, H., Rosemblatt, M., Valenzuela, P.D., 2005. Human and rodent humoral immune responses to Andes virus structural proteins. Virology 334, 319–326.
Vaheri, A., Henttonen, H., Voutilainen, L., Mustonen, J., Sironen, T., Vapalahti, O., 2013a. Hantavirus infections in Europe and their impact on public health. Rev. Med. Virol. 23, 35–49.
Vaheri, A., Strandin, T., Hepojoki, J., Sironen, T., Henttonen, H., Makela, S., Mustonen, J., 2013b. Uncovering the mysteries of hantavirus infections. Nat. Rev. Microbiol. 11, 539–550.
Vaheri, A., Strandin, T., Hepojoki, J., Sironen, T., Henttonen, H., Mäkelä, S., Mustonen, J., 2013c. Uncovering the mysteries of hantavirus infections. Nat. Rev. Microbiol. 11, 539–550.
de Vries, E., Tscherne, D.M., Wienholts, M.J., Cobos-Jimenez, V., Scholte, F., Garcia-Sastre, A., Rottier, P.J., de Haan, C.A., 2011. Dissection of the influenza A virus endocytic routes reveals macropinocytosis as an alternative entry pathway. PLoS Pathog. 7, e1001329.
Yamauchi, Y., Greber, U.F., 2016. Principles of Virus Uncoating: cues and the Snooker ball. Traffic.